

Shear localization in quasi-two-dimensional frictionless hydrogel layer controlled by packing fraction and system geometry

Yuto Sasaki^{1,*} and Hiroaki Katsuragi¹

¹Department of Earth and Space Science, University of Osaka, 1-1, Machikaneyama, Toyonaka, Osaka, 5600043, JAPAN

Abstract. How do packing fraction and system geometry affect shear banding, which controls the entire system's rheological properties? In this study, we demonstrate that both increases in packing fraction and in shear channel width decrease shear band width, leading to shear localization. We conducted shear experiments on a hydrogel granular layer floating on a liquid surface in a Couette cell. A relationship between torque and rotation rate was measured and in-situ particle motions were recorded at packing fractions of 0.6–0.8 and channel width normalized with particle size of 9–33. A sudden formation of a shear band was captured at the initial yielding point. At the steady state, we tracked each particle's motion and quantified the velocity field. Based on the velocity distribution, the measured shear band width exhibits a decrease with channel width. This system-geometry-induced localization simply depends on channel width regardless of strain rate. High packing fraction also causes the shear localization. We also measured the flow law of the granular layer. It demonstrates the typical transition with strain rate from constant stress yielding to viscous flow. However, the shear band width is not affected by the regime transition from yielding to viscously flowing.

1 Introduction

Understanding the connection between local particle motions and bulk deformation properties (shear structure and constitutive law) is a fundamental challenge in both geophysics [1] and soft matter physics [2]. Despite extensive research, a long-standing unresolved question is what controls the shear localization structures of granular media, a phenomenon known as shear banding.

Shear banding is characterized by the spatial distribution of velocity. It varies widely and unexpectedly depending on system geometry, particle properties, and shear conditions, even using the typical Couette cell geometry [2, 3]. Especially, the packing fraction affects shear banding [4, 5] and the system size is also considered a key parameter controlling shear band width rather than particle size [6]. However, a comprehensive understanding of how these factors control the shear band width and its relation to the bulk rheological properties of granular media is still lacking. It would help control the powder manufacturing process and elucidate the physical mechanism of shear localization within granular flow.

In this study, we investigated the effects of packing fraction and Couette channel width on the shear band width. To bridge the gap between extensively explored bubble raft [4] and rigid dry particles [5], we studied the shear banding and flow law of soft and frictionless hydrogel particles floating on a liquid surface. The empirical law of shear band width is obtained, providing new insights into the governing mechanisms of shear localization.

2 Methods

We conducted shear experiments on a granular layer floating on a lubricating fluid surface. Using our newly developed Couette cell [7], a quasi-two-dimensional granular layer was sheared by the central rotating cylinder. The sidewalls of the cylinder and cell are covered with the same particles, namely Couette flow between the rough surfaces (note that runs #27, 29, and 30 in Table 1 were conducted in the cell with a smooth sidewall). As a Couette cell, we used a transparent acrylic cylindrical container.

To constrain the rheological constitutive law of this granular layer, the rotating rate was varied across 0.06–120°/s, corresponding to the strain rate of $\dot{\gamma} = 10^{-4}$ –5 /s depending on system size. The torque of the rotating cylinder and particle motions were recorded with a viscometer at 2 Hz and with a USB camera at 10 fps, respectively. Details of the experimental setup are described in [7].

2.1 Materials

We used spherical hydrogel particles with a diameter of $d = 4.3$ mm, which have low friction and low rigidity compared to typical glass beads. In addition to their low-friction nature, we floated them on a lubricating fluid surface without any basal friction. We limited the number of particles as the layer thickness is within the diameter of the particle to maintain a quasi-two-dimensional setup. This enables us to observe in-situ particle motions and shear banding phenomena by visually recording from the bottom of the transparent container. Before each experimen-

*Corresponding author: sasaki.geoscience@gmail.com

Table 1. Summary of experimental conditions.

Run #	w_{ch} (mm)	d_{cyl} (mm)	ϕ	$\dot{\gamma}$ (/s)
97	40	19	0.68	10^{-3} –5
27	43	19	0.77	10^{-3}
29	43	19	0.81	10^{-3}
30	43	19	> 0.81	10^{-3}
99	47	144	0.66	10^{-3} – 10^{-1}
106	66	19	0.66	10^{-3} – 10^{-1}
108	78	144	0.66	10^{-3} – 10^{-1}
102	110	19	0.66	10^{-3} – 10^{-1}
79	141	19	0.59	10^{-3} – 10^0
69	141	19	0.72	10^{-3}
83	141	19	0.80	10^{-4} – 10^0

tal run, we stirred up the floating particles to make them disperse randomly.

Using a transparent aqueous solution of sodium polytungstate, the granular layer can float on its surface. We set the solution concentration of 2.6–2.9 g/cm³ (corresponding viscosity $\sim 2 \times 10^{-2}$ Pa s). This density is just above the particle density of around 2.6 g/cm³ and makes a liquid surface nearly smooth, leading to a reduction of the surface tension. We also added 1 wt% of the surfactant of dish soap (sodium alkyl ether sulfate) to reduce the interparticle tension, which was applied only to runs at packing fractions of $\phi = 0.66$ –0.68 (Table 1). The solution depth was set to approximately 10 mm, more than the maximum thickness of laminar boundary layer of approximately 6 mm, calculated under viscous drag by the fastest rotation of a cylinder with a diameter of 19 mm at 120°/s.

2.2 Experimental conditions

We investigated the effects of packing fraction and system geometry on shear banding. The experimental conditions are summarized in Table 1. The packing fraction was varied across $\phi = 0.6$ –0.8, where the number of particles varies depending on the system size. The channel width w_{channel} normalized to particle diameter d was varied across 9–33, by using three cylindrical containers (outer sidewall) with diameter of 100, 150, 240, 300 mm and rotating cylinders (inner sidewall) with diameter of $d_{\text{cylinder}} = 19, 144$ mm. At each condition, we obtained the flow law from the measured stress τ and strain rate $\dot{\gamma}$, and quantified the shear band width w from the recorded binary images.

3 Results and Discussion

We investigated the temporal evolution of mechanical torque (Sec. 3.1) and shear banding with particle motions (Sec. 3.2) under various channel widths (Sec. 3.3) and packing fractions (Sec. 3.4). The obtained flow law $\tau(\dot{\gamma})$ is compared with the shear band width (Sec. 3.5).

3.1 Temporal evolution of mechanical response

Temporal evolution of torque in the granular layer typically shows the initial elastic deformation, subsequent yielding, transient and steady flow with stick-slip events,

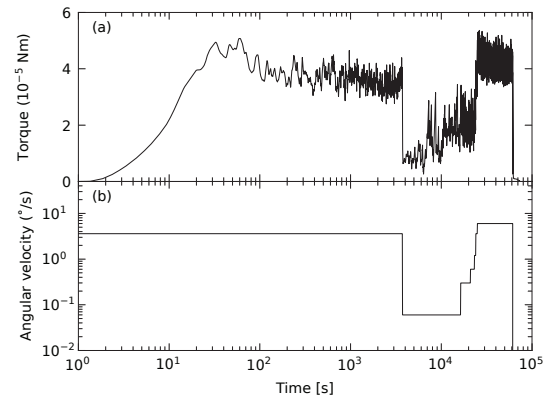


Figure 1. Example of experimental data in run #99. (a) Measured torque (N m) and (b) angular velocity (°/s) set for the motor with the rotating cylinder. After ~ 3500 s, the velocity was changed in a stepwise manner.

at a constant rotating rate (Fig. 1). On the yielding point, e.g., at ~ 30 s in Fig. 1, we captured the sudden formation of a shear band with cooperative particle motions from the initial homogeneous and random structure. Velocity step changes cause another transient flow and stick-slip phenomena with different periods.

3.2 Shear band structure

We tracked and quantified the particle motions using the particle tracking velocimetry with Open CV software functions [8]. Fig. 2a, b show the velocity field of the particles at $\dot{\gamma} = 10^{-3}$ /s and $\phi = 0.66$ in the system of $w_{\text{channel}} = 78$ and 47 mm, respectively. The velocity V of each particle is obtained by the difference between its positions over 100 s (1000 frames), and Fig. 2a, b demonstrate examples during specific 1000 frames under the steady state. Arrows indicate each particle’s velocity vectors and the background contours are obtained by linearly interpolating the data with a 300×300 grid, a spacing of approximately a quarter of the particle diameter.

Using the interpolated particle velocity field data, we obtained the radial distributions of particle velocity $V(r)$, with the radial distance from the cylinder center, r (Fig. 2c). It can be clearly seen that the faster shear zone is concentrated around the rotating cylinder surface ($r = d_{\text{cylinder}}/2$) with wider channel systems. This distribution was consistent at $\dot{\gamma} = 10^{-3}$ (Fig. 2c) and 10^{-1} /s.

Fig. 2c shows that the radial distribution $V(r)$ follows the exponential decay away from the cylinder surface, as $\exp(-r/\alpha)$ with a characteristic length α . The exponential decay of the particle velocity has been consistently recognized in soft bubbles [4] and frictional plant seeds or plastic beads [3, 9] under the Couette flow with some models.

Besides, in Fig. 2c, wider channel systems hold the wider outer creep region with distinctively slow decay of $V(r)$, resulting in shear localization. This creep region constrain the width of inner shear band by a deviation from the exponential decay of particle velocity. Such tailed exponential distributions have been reported previously for bi-dispersed photoelastic disks [5] and corresponding simulations [10] in the Couette geometry, and mono-dispersed

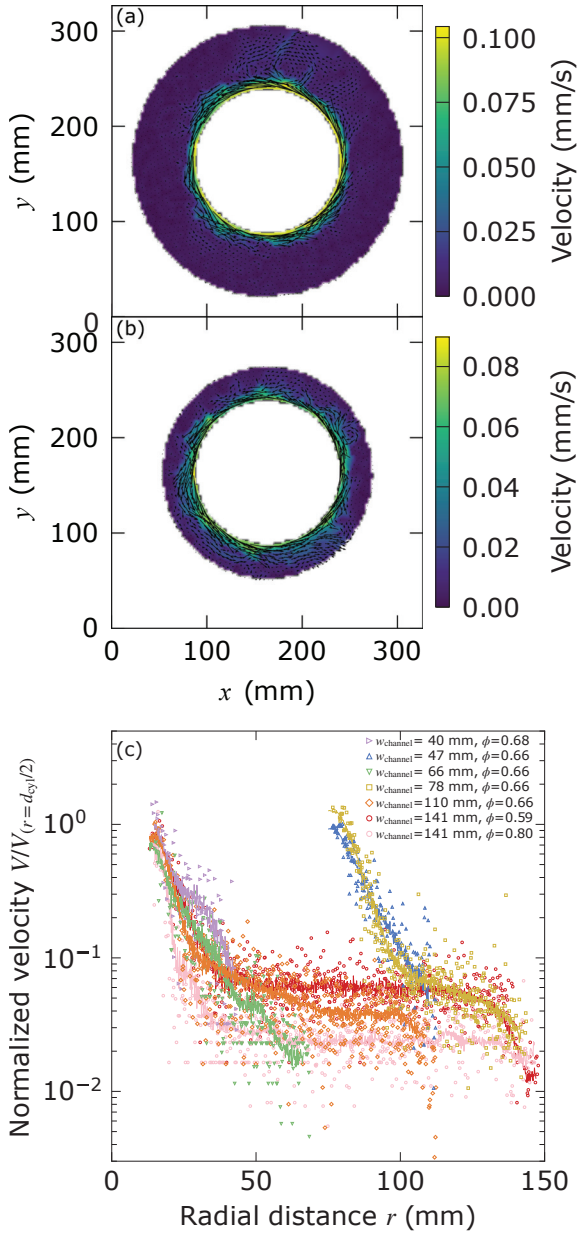


Figure 2. Radial profile of particle motions during specific 100 s in steady state at $\dot{\gamma} = 10^{-3} /s$. (a, b) Instantaneous particle velocity distributions at $w_{\text{channel}} = 78$ and 47 mm, respectively. The central cylinder rotates counterclockwise. Arrows are the velocity vector of each particle and background contours indicate their interpolated values. (c) Radial distribution of the velocity V normalized to the cylinder surface velocity $V_{(r=d_{\text{cyl}})}$ (symbols) and its interpolated field values (lines) at $\dot{\gamma} = 10^{-3} /s$ and various w_{channel} .

rigid glass beads in the ring shear geometry [6], although their physical origin remains unclear until today.

3.3 Effect of channel width

The shear band and channel widths can be related as shown in Fig. 3. We defined the shear band width as $w = 2.2\alpha$ with a characteristic decay length α , corresponding to the velocity decay by a factor of 10. α is obtained by the exponential fitting to the inner part of the radial profile in Fig. 2c. When we plot the measured shear band width normalized to the channel width, w/w_{channel} ,

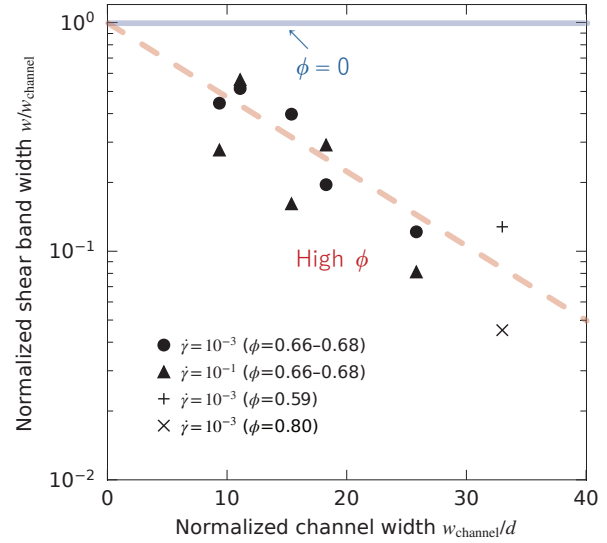


Figure 3. Relationship between shear band width and channel width. Data plots are at various $\dot{\gamma}$ and ϕ . The Newtonian solution should correspond to the blue line.

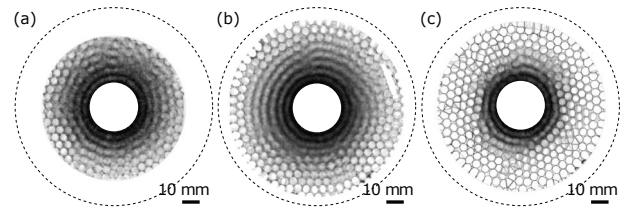


Figure 4. Effect of packing fraction on shear band width. (a–c) Time-lapsed differential images at $\phi = 0.77$ (#27), 0.81 (#29), and higher conditions (#30), respectively. Darker regions correspond to active particle motions. Dashed lines indicate the container sidewall, which is out of the camera’s field of view.

against the channel width normalized to the particle diameter, w_{channel}/d , another exponential relation is obtained with a weak dependence on $\dot{\gamma}$ and d_{cylinder} (Fig. 3). Contrary to purely Newtonian fluid ($\phi = 0$), higher ϕ potentially causes enhanced shear localization with wider channel geometry. Therefore, the effect of packing fraction is also a controlling factor of shear localization in addition to the channel width. These relationship can be expressed as $w = w_{\text{channel}} \exp(-\frac{w_{\text{channel}}}{d\lambda(\phi)})$ with a characteristic channel scale $\lambda(\phi)$.

3.4 Effect of packing fraction

We, thus, also investigated the effect of packing fraction. Fig. 4a–c are the time-lapse of 10-second-differential sequences of binary images at $\phi = 0.77$, 0.81 , and higher, respectively. All runs were conducted under the same geometry with $w_{\text{channel}} = 43$ mm and $\dot{\gamma} = 10^{-3} /s$. Note that the outer edge regions are not captured due to the refraction by the tapered edges of a container base, with dashed circles indicating the channel sidewall. In the larger system in run #83, we also found a similar shear localization with higher ϕ [7]. In the Couette cell, higher packing fractions are associated with stress concentration near the surface of the rotating cylinder, leading to the shear band formation.

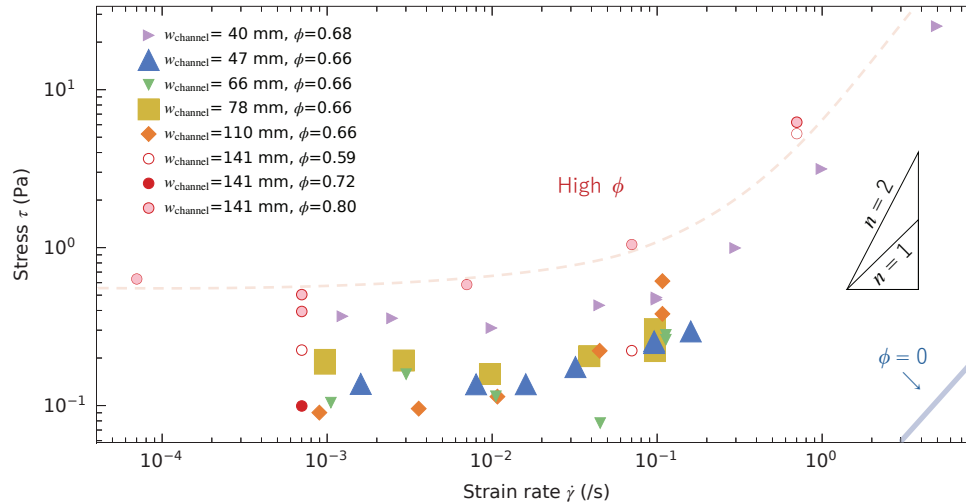


Figure 5. Flow law of the floating granular layer. The relationship between strain rate $\dot{\gamma}$ and stress τ is plotted in a log-log scale. Each pair of symbol and color corresponds to the same w_{channel} and ϕ . Larger symbols mean the larger $d_{\text{cylinder}} = 144$ mm. A blue line indicates the linear viscosity (2×10^{-2} Pa s) of the pure interparticle solution.

3.5 Flow law (effect of strain rate)

To clarify the microscopic deformation process, we investigated the flow law, the relationship between shear stress τ and strain rate $\dot{\gamma}$ under the steady state. Fig. 5 exhibits a transition at $\dot{\gamma} \sim 10^{-1}$ /s from solid-like behavior with constant yield stress τ_0 to flow behavior, following the Herschel-Bulkley model or $\mu(I)$ rheology with the inertial number I [11] as $\tau = \tau_0 + k\dot{\gamma}^n$ ($n \sim 1.3$ in this study) with a constant k . Packing fraction ϕ modifies these flow law parameters (ref. [7]). Surprisingly, the channel width w_{channel} weakly affects the flow law of the bulk system, although it controls the local shear band width w at $\dot{\gamma} = 10^{-3}$ and 10^{-1} /s. This means that the shear band width relation $w(w_{\text{channel}}, \phi)$ (Fig. 3) seems to be maintained regardless of the strain rate, namely, the microscopic deformation mechanisms: yielding or viscous flow (corresponding to I). To further ensure this universality, experiments under varied conditions are needed, as the current parameter ranges of w_{channel} , ϕ , $\dot{\gamma}$ are still limited.

Our results of shear band width variations with the exponential distribution of velocity remain valid across various conditions: flow law regimes in this study, and also particle frictions, rigidities, system dimensions in the previous studies (Sec. 3.2). This suggests that the shear band structures are controlled by shear channel width and packing fraction, regardless of the details of deformation mechanism. This insight leads to the advancement in physically interpreting geological shear zone structures as an indicator of porosity and effective tectonic-fault thickness.

4 Conclusions

We investigated the effects of channel width and packing fraction on the shear band width. By experimentally shearing a soft hydrogel granular layer, both channel width and packing fraction cause the shear localization, while the former has little effect on the flow law. The radial distribution of shear follows a tailed exponential function, the physical origin of which requires further investigation.

Acknowledgment

This work was supported by the Sasakawa Scientific Research Grant from the Japan Science Society 2024-6006 funded to Y. S., and by JSPS KAKENHI Grant Number JP24H00196 funded to H. K.

References

- [1] H. Fossen, G.C.G. Cavalcante, Shear zones – a review, *Earth-Science Reviews* **171**, 434 (2017).
- [2] P. Schall, M. Van Hecke, Shear bands in matter with granularity, *Annual Review of Fluid Mechanics* **42**, 67 (2010).
- [3] GDR MiDi, On dense granular flows, *The European Physical Journal E* **14**, 341 (2004).
- [4] G. Debrégeas, H. Tabuteau, J.M. Di Meglio, Deformation and Flow of a Two-Dimensional Foam under Continuous Shear, *Physical Review Letters* **87**, 178305 (2001).
- [5] D.W. Howell, R.P. Behringer, C.T. Veje, Fluctuations in granular media, *Chaos: An Interdisciplinary Journal of Nonlinear Science* **9**, 559 (1999).
- [6] J.C. Tsai, J.P. Gollub, Granular packings sheared in an annular channel: Flow localization and grain size dependence, *Physical Review E* **72**, 051304 (2005).
- [7] Y. Sasaki, H. Katsuragi, Origin of slow earthquake statistics in low-friction soft granular shear, *arXiv* (2025), 2502.01355.
- [8] G. Bradski, The OpenCV Library, *Dr. Dobb's Journal of Software Tools* **4** (2000).
- [9] H.T. Fabich, T.I. Brox, D. Clarke, J.D. Seymour, S.L. Codd, P. Galvosas, J. Brown, A.J. Sederman, D.J. Holland, Measurements of the velocity distribution for granular flow in a Couette cell, *Physical Review E* **98**, 062901 (2018).
- [10] S. Schöllmann, Simulation of a two-dimensional shear cell, *Physical Review E* **59**, 889 (1999).
- [11] P. Jop, Y. Forterre, O. Pouliquen, A constitutive law for dense granular flows, *Nature* **441**, 727 (2006).